THE DEFORMATION OF A VORTEX SHEET BEHIND A SWEPT BACK WING; COMPARISON OF MEASUREMENTS AND CALCULATIONS. +)

Th.E. Labrujère and O. de Vries

National Aerospace Laboratory NLR, Amsterdam, The Netherlands.

Abstract

The deformation of a vortex sheet behind a 30 degrees swept back wing, has been measured in a low-speed wind tunnel.
The measurements included:
- A total-head survey behind the wing,
- Sidewash measurements across the wake,
- Measurements of trailing vorticity by a vortex indicator.

It has been found, that 60 percent of the trailing vorticity is concentrated in the tip vortex leaving the wing tip upper surface. Proceeding downstream, the remaining vorticity due to the wing diffuses into the surrounding air, without rolling-up into the tip vortex.

The deformation of the vortex sheet behind the wing has been calculated by means of a method, which may be considered as an extension of the NLR panel method for the determination of the pressure distribution on lifting wing-body combinations in uniform flow. It comprises an iterative procedure for the determination of the location of the vortex sheet, represented by discrete vortices, for given onset flow conditions. The diffusing process and the presence of a concentrated tip vortex are not taken into account in the calculation method.

In view of the above mentioned simplifications, the agreement between calculation and experiment may be considered satisfactory.

Symbols

α = angle of attack, measured relative to the root chord (degrees)
Γ = circulation (m^2/sec)
Γ_{th} = circulation, measured with an "ideal" vortex indicator
δ = sidewash angle (degrees)
$\Delta\delta$ = maximum difference of the sidewash angle just below and above the wake (degrees)
ω = rotational speed of the vortex indicator (radians/sec)
b = wing span (m)
c = wing chord (m)
$C_L = \frac{\text{lift}}{q_o b c}$ = total lift coefficient (-)
$c_\ell = \frac{\text{section lift}}{q_o c}$ = section lift coefficient (-)
$C_p = \frac{p-p_o}{q_o}$ = pressure coefficient (-)
D = diameter of the vane wheel of the vortex indicator (m)
H = total head (kgf/m^2)
p = local static pressure (kgf/m^2)
p_o = free-stream static pressure (kgf/m^2)
q_o = free-stream dynamic pressure (kgf/m^2)
Δu = sidewash velocity difference across the vortex sheet (m/sec)
V_o = free-stream velocity (m/sec)
x = co-ordinate along the local chord; x=0 at the leading edge, (m)

or

downstream co-ordinate along the free stream direction; x=0 at the trailing edge of the tip section (m)
y = spanwise co-ordinate; y=0 at the tip (m)
z = vertical co-ordinate; z=0 at the trailing edge of the tip section (m)

1. Introduction

Potential flow calculations around wing-body combinations often assume a straight vortex sheet behind the wing, extending to infinity in a fixed direction. However, the deformation and rolling-up of the vortex sheet can have a significant effect, especially on downstream aircraft components, e.g. tail surfaces and could possibly also influence the pressure distribution on the wing.

A number of investigators has calculated the deformation of a vortex sheet by discretizing the continuous vortex sheet by a number of discrete vortices [1,2,3,4]. Also at NLR, a program has been developed [5,6], which calculates the vertical displacement and, approximately, the rolling-up of the vortex sheet. This program may be considered as an extension of the NLR panel method [7] for the determination of the pressure distribution on lifting wing-body combinations.

Apart from numerical questions as e.g. the convergence to a well-defined limit, the question

+) This investigation was performed under contract with the Netherlands Agency for Aerospace Programs (NIVR).

arises whether the calculated results agree with the actual flow field behind a wing. Experimental data on vortex sheet deformation, suitable for comparison with theoretical results, can hardly be found in the literature. Therefore, a wind tunnel investigation was started to measure the downstream development of the vortex sheet behind a swept back wing and the spanwise lift distribution on the wing[8].

In this presentation, model geometry, lift distribution at two angles of attack and a survey of the downstream development of the vortex sheet, will be given. The results of the measurements will be compared with the results calculated with the NLR method.

2. Model

The model consists of a 30 degrees swept back wing of constant chord and a NACA 0012-64 profile parallel to the plane of symmetry (figure 1). The wing has a washout of 4°, linearly distributed along the span. The tip consists of one half of a body of revolution, generated by rotating the tip profile about its chord line.

The starboard half of the wing is provided with pressure holes in 15 sections parallel to the plane of symmetry and also in 5 sections on the tip, perpendicular to the plane of symmetry (figure 1).

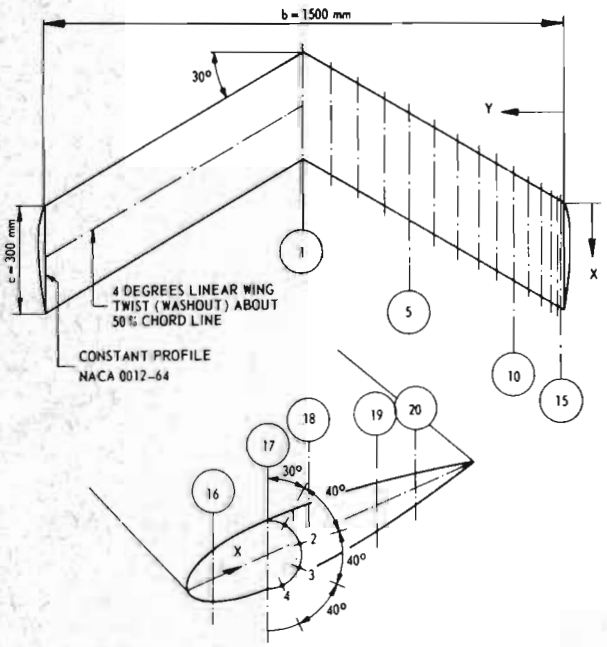

Fig.1 Wing geometry, locations of the sections with pressure holes and a detail of the pressure holes in the wing tip.

The sting mounted model was suspended in an inverted position in the octagonal test-section (width 3 m, height 2 m) of the low-speed wind tunnel (figure 2). The junction between wing and sting was placed at the wing lower surface, to restrict the disturbance by the sting. The junction was placed asymmetrically, to permit pressures to be measured at the wing root.

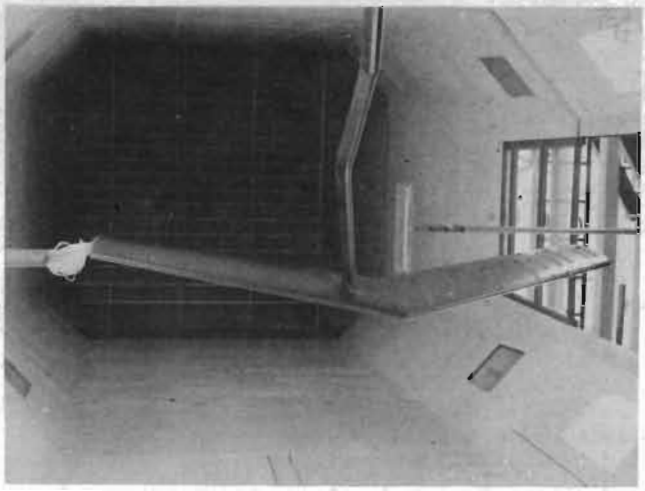

Fig.2 Sting mounted model, suspended in an inverted position. Notice the asymmetrically placed sting, the pressure leads at the port wing tip and the total head rake behind the starboard wing.

3. Testing techniques

3.1 Introductory remark

The lift distribution on the wing was determined from pressure measurements. Some insight into the flow characteristics on the wing surface was obtained by flow visualization techniques, i.e. tufts and oil patterns.

The experimental determination of the development of the vortex sheet behind the wing, will be discussed hereafter in some detail.

3.2 Total-head survey

By considering the total-head loss, originating in the boundary layer of the wing, as a passive quantity flowing downstream, a total-head survey at several downstream stations behind the wing, should reveal the streamline pattern behind the wing.

The total-head distribution was measured with a total-head rake (cf. figure 2) at several spanwise and downstream stations. By interpolation, contour lines of constant total head, in planes perpendicular to the free-stream, can be determined. The down-stream deformation of the contour lines shows the cross-flow streamline-pattern. However, the wake diffuses downstream and the determination of the contour lines becomes increasingly inaccurate. The location of the trailing vorticity within the wake cannot be determined by this technique.

3.3 Sidewash measurements

In potential flow, the sidewash varies discontinuously across a vortex sheet. In viscous flow, the trailing vorticity occupies a layer with finite thickness and the sidewash varies through this layer with a finite gradient.

Measuring the sidewash with a yaw meter at several downstream stations gives, in principle, the possibility to determine the location of this

layer with trailing vortioity. Moreover, the magnitude of this sidewash is a measure of the local strength of the trailing vortioity and offers a possibility to oheck the usefulness of the prediotion of the flow field behind a wing by numerical oaloulations.

The sidewash has been measured with a oobra head type of yaw meter, which was used as a remotely controlled null-reading device. The angular aoouracy was about 1/4 degree and possibly a somewhat larger systematic error of about 1 degree was present (calibration of free-stream direotion with model in the test section).

At a fixed spanwise and downstream looation, the yaw meter was transversed vertioally. The acouracy of the vertioal traverse is about 2 mm, but there are possible systematio errors in vertioal position, due to the deflection of the support of the yaw meter oontrol box under aerodynamio load. Therefore, the determination of the location of the vorticity layer from widewash measurements is not suffioiently aocurate. Moreover, a traverse in a potential flow at some distance of a concentrated vortex shows a large sidewash gradient. This indicates that a sidewash gradient not always means that the yaw meter traverse crossed a layer of trailing vorticity.

With the above mentioned exoeption, it is possible to determine the strength of the trailing vortioity from the maximum differenoe in sidewash aoross the wake ($\Delta\delta$). The trailing vorticity $d\Gamma/dy$ induoes a sidewash velocity difference Δu just below and above the trailing vortioity layer. Assuming a constant mean velocity above and below the wake equal to V_o, the difference in sidewash angle aoross the wake can be oalculated from:

$$\Delta\delta = \frac{\Delta u}{V_o} = \frac{d\Gamma/dy}{V_o} \qquad \text{(radians)}$$

3.4 Measurement of trailing vorticity

The direot measurement of the trailing vortioity appears to be the only way to determine the location of this trailing vorticity and the development of the rolling-up process properly.

In order to obtain a quick but approximate method for measuring the trailing vorticity in the wake, a so-called "vortex indicator" was chosen.

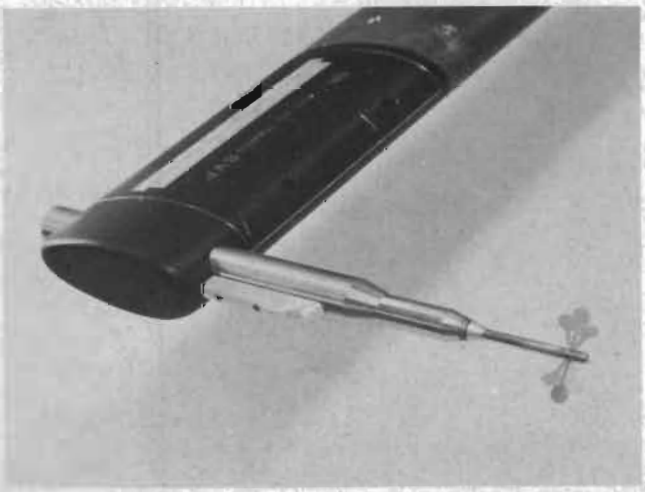

Fig.3 Vortex indioator mounted in a streamlined support.

The vortex indicator (developed at NLR) consists of a small wheel with vanes parallel to the axis of the wheel. The axis of the wheel is plaoed parallel to the mean flow. Only when the flow through the vane wheel oontains vorticity with its axis parallel to the mean flow, the vane wheel will rotate.

A low friction, cruoial for the proper operation of the instrument, has been obtained by applying air-bearings. The number of revolutions of the vane wheel has been measured, without extracting energy from the wheel, by a light souroe and a photo-diode, built into the instrument. Vane wheels of different diameters oould be used. A photograph of the vortex indicator is shown in figure 3.

Aooording to a simple analysis[8], the relation between the rotational speed ω and the circulation Γ_{th} enolosed by the vane wheel, should be:

$$\Gamma_{th} = \frac{\pi}{4} D^2 . 2\omega$$

Tests with the vortex indioator showed, however, that aocurate calibration was impossible, but a very rough oalibration factor has been extracted from the tests, viz.:

$$\Gamma = 0.7\ \Gamma_{th}$$

4. Numerioal method

The numerioal method for the calculation of the deformation of the vortex sheet behind a wing, is an extension of the NLR panel method[7]. This is a singularity method, using source distributions on the contour and horseshoe vortices inside the wing. The vortex lines extend to infinity on a discontinuity surfaoe behind the wing.

The method[5], that has been used for the determination of the location of the vortex sheet behind the wing, proceeds along the following lines:

- For an estimated position of the vortex sheet, the lift distribution on the wing is caloulated (first step).
- With the lift distribution thus determined and the strengths of the vortices thus being known, the trailing vortioes are relaxed into the local streamline directions. In this relaxation proocedure, the modification of the streamline pattern by modifying the shape of the vortex lines, is taken into account.
- For the newly found shape of the vortex sheet, the lift distribution on the wing is determined again (seoond step), whereafter the whole proocedure is reiterated until convergence of the results has been established.

Full details of the method may be found in referenoes[5,7], but here it may suffice to make the following remarks:

- No attempt has been made to represent the tip edge separation, that may lead to the formation of the tip vortex, leaving the wing some distanoe upstream from the trailing edge.
- The velocity distribution along the vortex sheet is calculated midway between the discrete vortices, for reasons of mathematical consistency.

The average flow angle at the discrete vortices themselves, is obtained by interpolation.

- The relaxation of the vortices is performed simultaneously while proceeding downstream, thus determining successive cross-sections of the vortex sheet in planes normal to the plane of symmetry of the wing.

5. Experimental results

5.1 Lift distribution

The lift distribution, determined from pressure measurements, is given in figure 4. Flow visualization indicated a crescent shaped area with flow separation at $\alpha = 16^{\circ}$ (C_L=0.82), whereas at $\alpha = 10^{\circ}$ (C_L =0.50), the flow is attached along the entire trailing edge.

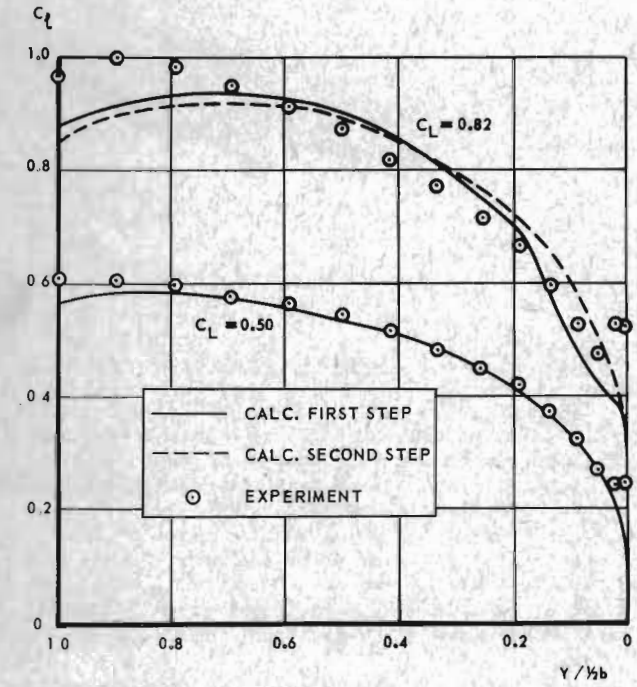

Fig.4 Measured and calculated spanwise lift distribution.

5.2 Wake deformation

Figure 5 gives an example of the deformation of the wake at several distances downstream (x=y=z=0 coincides with the wing tip trailing edge).

Some remarks can be made about this figure, viz.:

- The tip vortex exists already at the wing tip trailing edge (x/c=0). Downstream, the vortex core moves slightly inboard and upwards. The upward movement is possibly caused by tunnel wall constraint.
- Downstream, the inboard part of the wake moves downwards. In the tip region, the wake stretches laterally and moves in a helical path around the tip vortex.
- The downstream broadening (diffusion) of the wake is not clear from this figure, because the contour lines are given at a constant value of the total head instead of a constant fraction of the maximum total head loss in the wake.

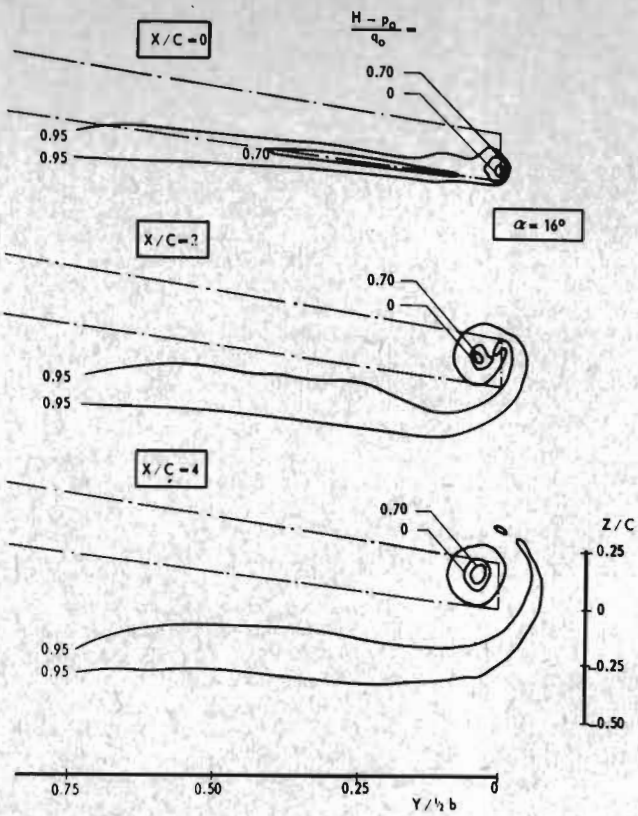

Fig.5 Contour lines of constant total head in planes perpendicular to the free-stream. The wake location is not corrected for tunnel wall constraint.

5.3 Sidewash across the wake

The sidewash variation in vertical traverses through the wake, is shown in figure 6. The large gradient of the sidewash is clearly shown. Downstream, the inboard stations show a diminuation of the gradient by diffusion of the vorticity. Close to the tip (2y/b = 0.07), the gradient of the sidewash increases downstream, due to the inboard movement of the tip vortex.

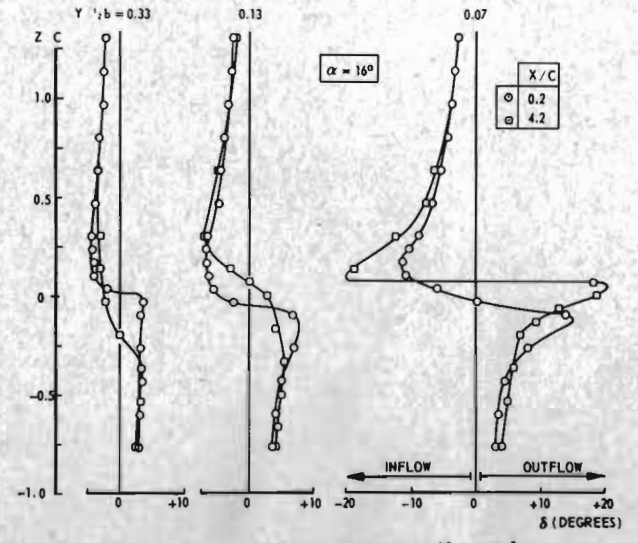

Fig.6 Sidewash variation across the wake, measured at 3 spanwise and 2 downstream stations.

The downstream variation of the spanwise distribution of the sidewash difference across the wake $\Delta\delta$ (see Sect. 3.3) is shown in figure 7. At $\alpha = 10^0$, there is no significant downstream variation. The downstream increase of $\Delta\delta$ in the tip region at $\alpha = 10$ and 16^0, is due to the inboard movement of the tip vortex (cf. Fig.6). At $\alpha = 16^0$, there is a downstream decrease of the strength of the trailing vorticity, which is possibly connected with the flow separation on the trailing edge at that angle of attack.

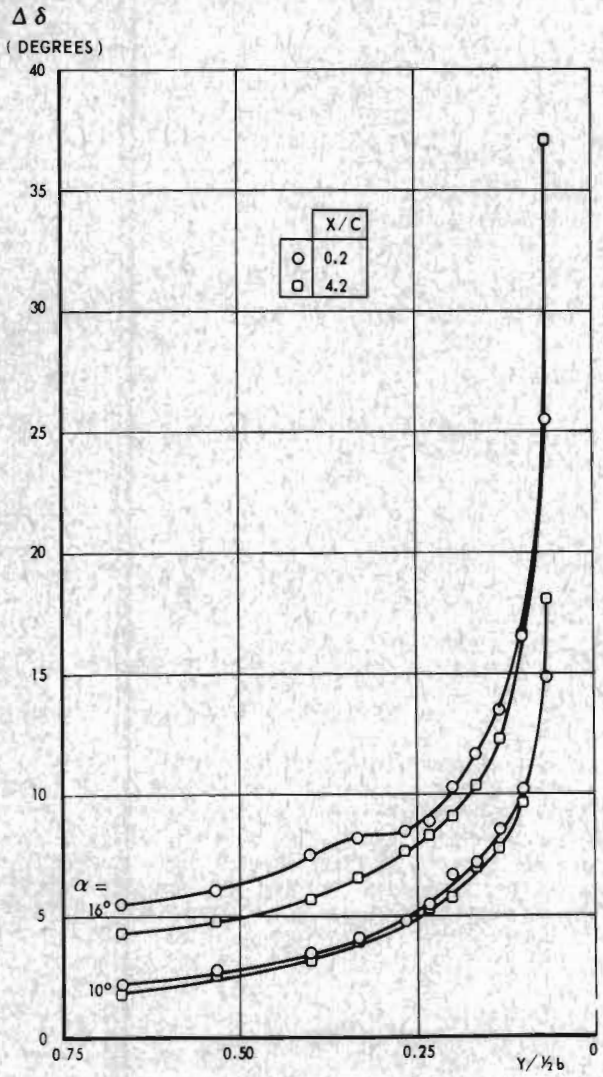

Fig.7 Sidewash difference across the wake, showing the downstream variation of the strength of the trailing vorticity.

5.4 Trailing vorticity

The location of the layer with trailing vorticity is determined by measuring at each spanwise station the vertical co-ordinate z, at which the vortex indicator showed the maximum rotation. Figure 8 shows the downstream development of the trailing vorticity layer, measured in that way. The last experimental point in the tip region coincides with the centre of the tip vortex.

Figure 9 shows the downstream variation of the strength of the trailing vorticity ($d\Gamma/dy$) in dimensionless form), using a rough estimate of the calibration factor of the vortex indicator. The

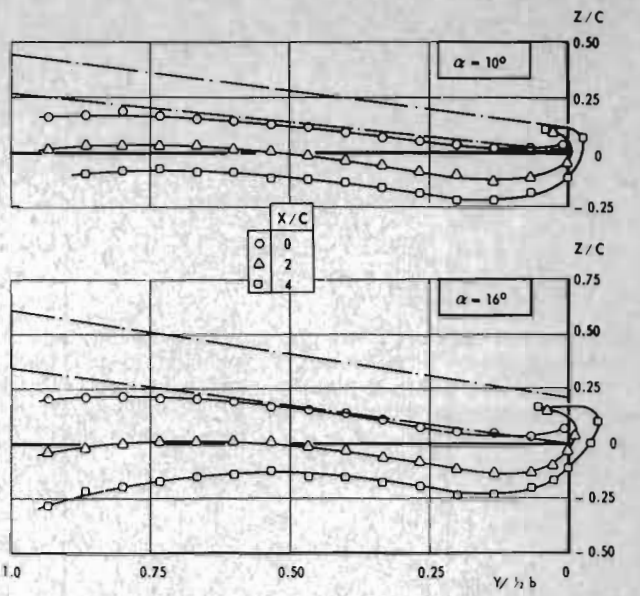

Fig.8 Location of the trailing vorticity layer, measured with the vortex indicator. The location is not corrected for tunnel wall constraint.

strong decrease with x/c in the tip region indicates the lateral stretching of the vorticity layer into a helical path around the tip vortex (cf. Fig.5). The apparent downstream decrease along the entire span is possibly caused by outward diffusion (widening) of the vorticity layer, so that the vane wheel of the indicator does no longer encompass all the vorticity of a definite spanwise part of the layer. It must also be noticed, that the plane of the measurements is perpendicular to the plane of symmetry of the wing.

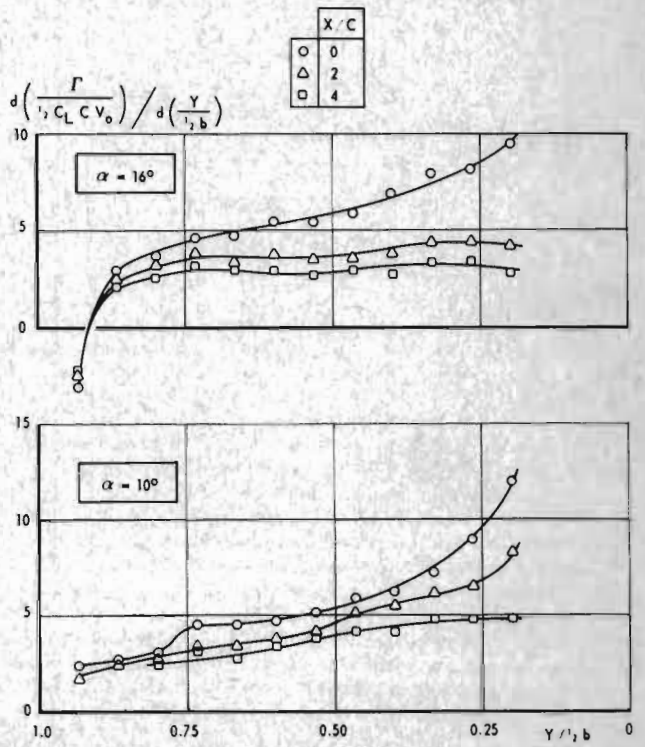

Fig.9 Spanwise distribution of the strength of the trailing vorticity, measured with a vortex indicator.

Therefore, due to the sweep of the wing, the distance from the trailing edge is larger at the root than at the tip.

It is interesting to know, whioh part of the circulation is contained in the tip vortex, already existing at the trailing edge and which part is contained in that part of the vortex sheet, that rolls-up into the tip vortex downstream.

The oiroulation on the wing can be estimated from the local wing lift c_l , using V_o instead of the local velocity at the bound vorticity (it has been ohecked with numerical calculations, that the error is within 5 percent). The strength of the tip vortex can be estimated from vortex indicator measurements.

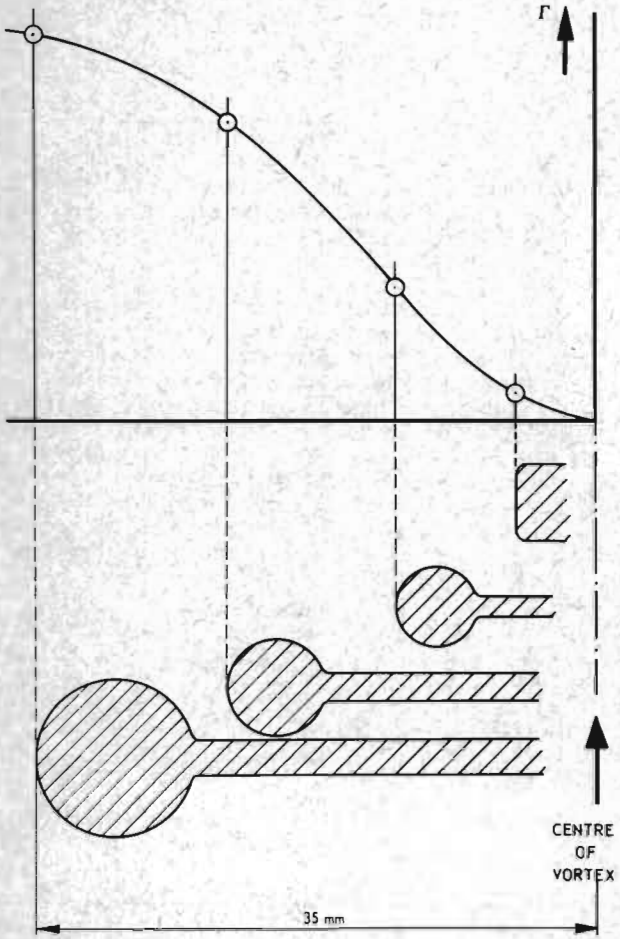

Fig.10 Sketch of different vane wheels for determining the circulation distribution of the tip vortex. Axis of vane wheel coincides with centre of vortex.

The vorticity in the tip vortex is distributed over a finite cross-sectional area. A vortex indicator, whose axis coincides with the centre of the tip vortex, will only measure that part of the circulation, that is enclosed by the vane wheel. Using different vane wheel diameters, the circulation distribution within the vortex can be determined (see Fig. 10), tending to a constant value of Γ at larger distance from the centre.

Figure 11 shows the circulation distribution in the tip vortex at three downstream stations. The arrows on the abscissa indicate the centres of the tip vortex at different x/c (tip vortex

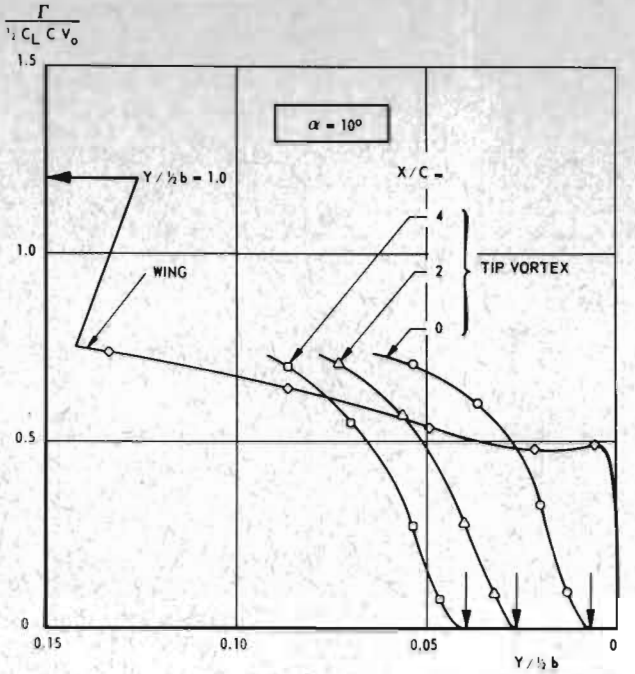

Fig.11 Downstream variation of the vorticity distribution in the tip vortex and the spanwise circulation distribution on the wing in the tip region.

moves inboard at increasing x/o). At small distances from the centre of the vortex, the circulation diminishes slightly downstream, revealing some vortex decay. At large distances from the oentre (maximum vane wheel diameter), no decrease is found.
From the shape of the circulation distribution a slight tendency of further increase of the oirculation could be detected.

The almost constant strength of the tip vortex along its downstream path, stands in marked contrast with the deorease of the strength of the vortex sheet in the tip region, shown in figure 9. Further measurements with the vortex indicator showed, that due to the lateral stretching along a helical path around the tip vortex, a rapid diffusion prevented this vorticity to be included into the core of the tip vortex.

Also shown in figure 11, is the circulation distribution on the wing in the tip region, determined from pressure measurements. The arrow on the ordinate indicates the maximum circulation at the wing root. It is clear from this figure, that already 60 percent of the total trailing vorticity is concentrated in the tip vortex at the wing trailing edge (x/c=0), whereas further downstream, the strength of the tip vortex hardly increases (within the range of the present tests). Measurements at large distances behind a wing[9] also showed, that a tip vortex contains about 60 percent of the maximum circulation, which agrees with the present measurements at short distances behind the wing.

Figure 12 suggests a possible course of bound and trailing vortex lines. It can be shown by Stoke's law, that the circulation of the tip vortex just behind the trailing edge must be equal to the circulation around wing section A.

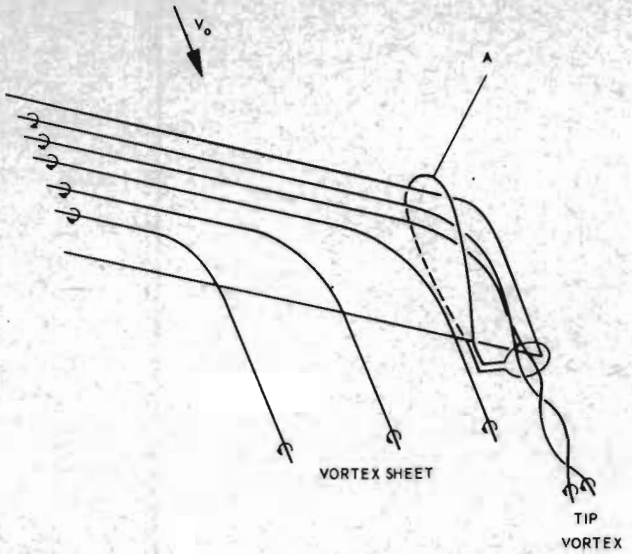

Fig.12 Bound and trailing vortices. Section A has a circulation equal to the tip vortex.

Figure 11 shows, that this section is located at 10 to 15 percent of the semi span from the tip. The viscous forces in the separated boundary layer on the tip have to be very effective in concentrating the vorticity into this tip vortex.

6. Comparison with calculations

6.1 Introductory remarks

Due to viscous and tunnel wall effects, there will be differences between experimental and calculated results. In potential flow, the same lift will be obtained at a lower angle of attack than in viscous flow and it seems obvious to compare experimental and calculated results at equal over-all lift, instead of at equal angle of attack, because the lift fixes the strength of the trailing vortex sheet and the perturbation of the free-stream, which determines the deformation of the vortex sheet. It means, however, that the wing position in space differs in calculation and experiment and this affects the downstream location of the vortex sheet in both cases.

The tunnel wall correction on angle of attack is nog needed, when experiment and calculation are compared at equal over-all lift. However, a correction on the downwash behind the wing is still necessary. Due to the approximate nature of the corrections found in the literature, these corrections are only estimated in a single case (detailed calculations with the NLR panel methodewere not considered worthwhile, because the calculated corrections will not differ largely from the estimated values).

6.2 Lift distribution

Figure 4 shows the calculated and measured spanwise lift distribution. The calculation with the a priori chosen vortex sheet location is designated with "first step", whereas the "second step" is the calculation with the deformed vortex sheet location.

The agreement between calculation and experiment is very good at $C_L = 0.50$. It must be noticed, that the agreement is good because almost equal over-all lift was chosen in both cases, in that way approximately compensating the viscous lift loss. Small deviations at tip and root are possibly caused by boundary layer displacement effects.

The less good agreement at $C_L = 0.82$ is probably caused by trailing edge separation (cf. Sect. 5.1). The relatively large difference in the tip region between first and second step, is possibly connected with the chosen distribution of discrete trailing vortices (panel distribution). At $C_L = 0.50$ no difference in shape was found between first and second step, because of a finer panel distribution at the tip was chosen in that case. The influence of the deformed vortex sheet on the over-all lift (second step), was only 3 percent.

6.3 Pressure distribution

Figure 13 shows the calculated and measured pressure distribution at two spanwise stations at $C_L = 0.82$. At mid semi span, the calculated

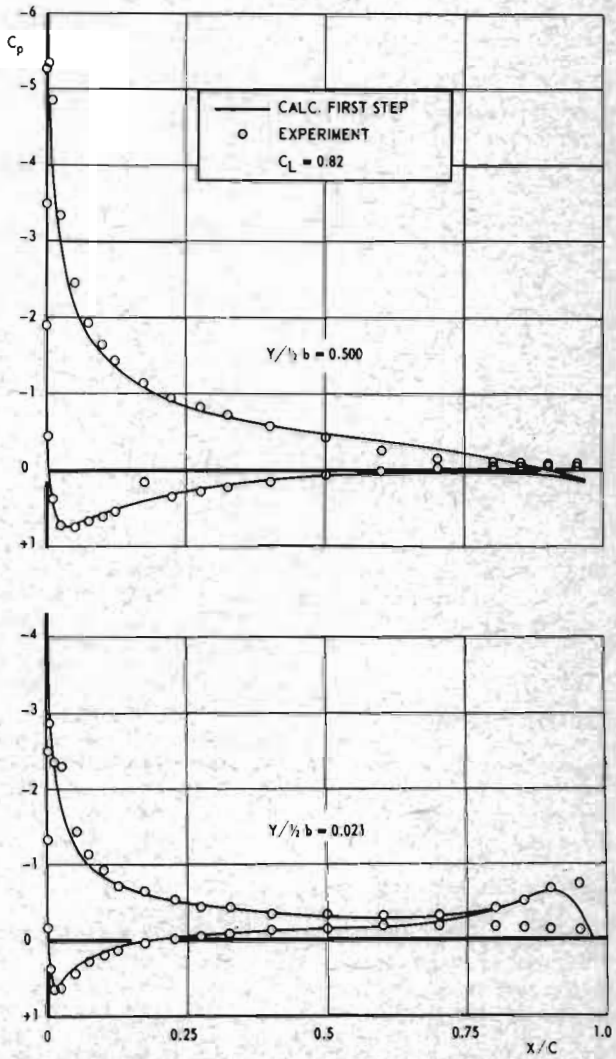

Fig.13 Measured and calculated chordwise pressure distribution at two spanwise stations.

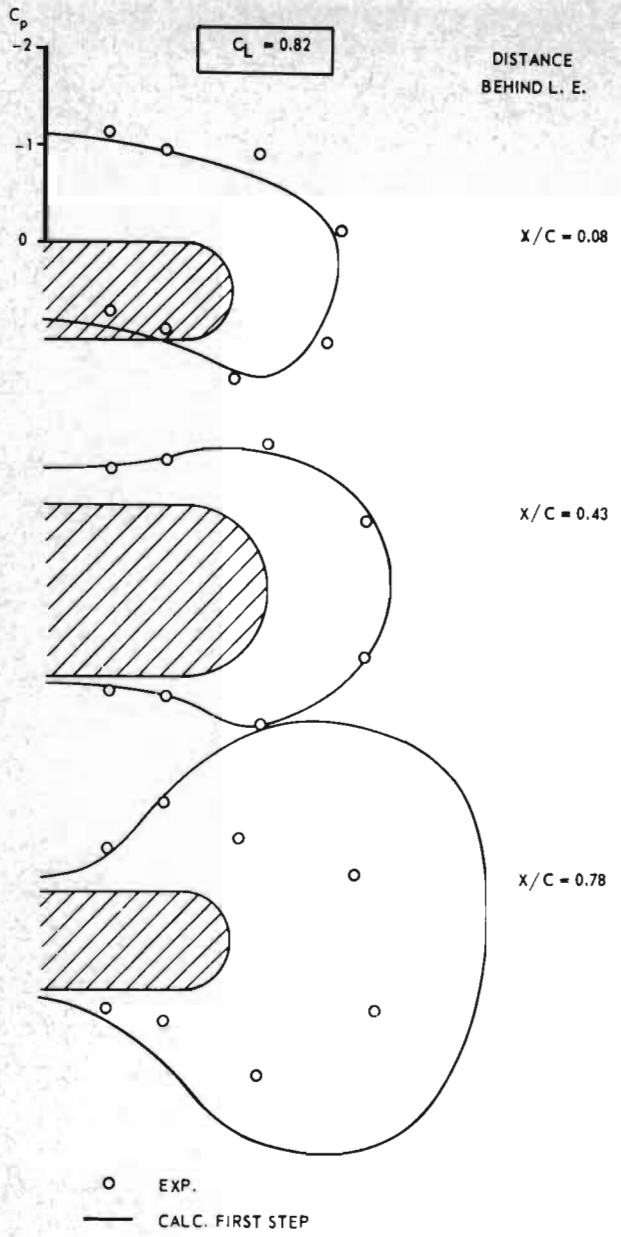

Fig.14 Measured and calculated pressure distribution in sections perpendicular to the tip chord.

pressure distribution agrees with the measured one, except on the rear part of the upper surface, where the influence of the flow separation is clearly visible. Even close to the tip, the agreement between calculation and experiment is very good, except on the rear part of the profile. This is possibly connected with the tip vortex on the wing tip upper surface.

The calculated and measured pressure distributions across the wing tip, are shown in figure 14. The agreement between calculation and measurement is very good at sections perpendicular to the tip chord, some distance away from the trailing edge. Close to the trailing edge (x/c = 0.78), large deviations occur. This is probably caused by the simple mathematical model for the tip flow, used in the calculations.

6.4 Vortex sheet location

Calculation and measurement have been performed at almost equal lift, which means different angles of attack in both cases. Due to the sweep back of the wing, the position in space of the trailing edge also differs. In order to compare the calculated vortex sheet location with the measured one, the wings have been shifted in such a way, that both wing tip trailing edges coincide ($x=y=z=0$), but there remains a difference in trailing edge position, increasing towards the wing root.

Figure 15 shows the vortex sheet location at two values of C_L and three downstream stations. At high lift, the calculated shape of the vortex sheet agrees better with the measured shape, than at low lift, as far as the rolling-up process is concerned. The increased downwash in the inboard region at C_L = 0.82, is not revealed by the calculations, possibly because of the limited number of trailing vortices used in the calculations and the lower lift at the root.

Figure 16 shows the measured and calculated downstream vortex sheet location at mid semi span. The difference in vertical and downstream scale must be noted. Also indicated is the position of the wing trailing edge during the measurements and the position used in the calculations.

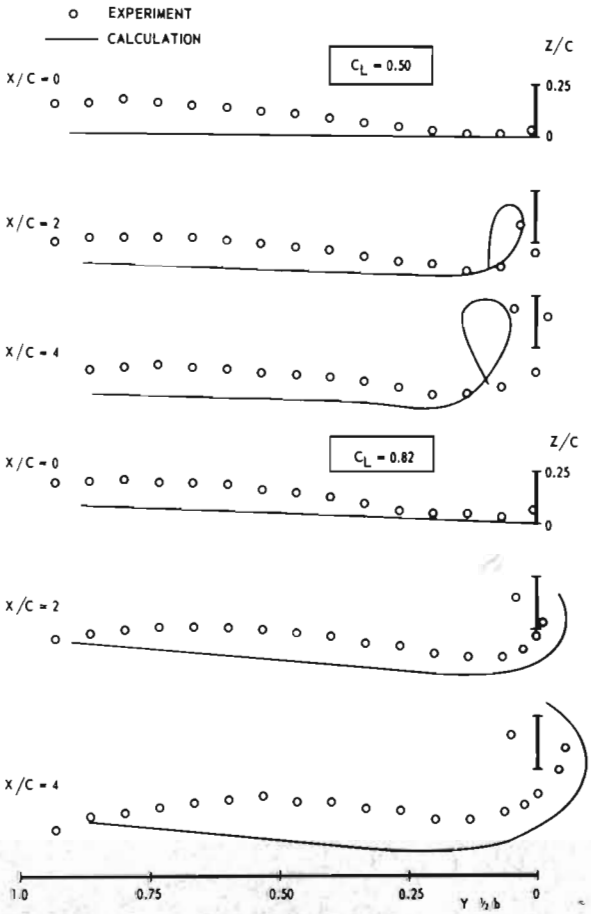

Fig.15 Measured and calculated spanwise vortex sheet location at 3 downstream stations and 2 C_L values.

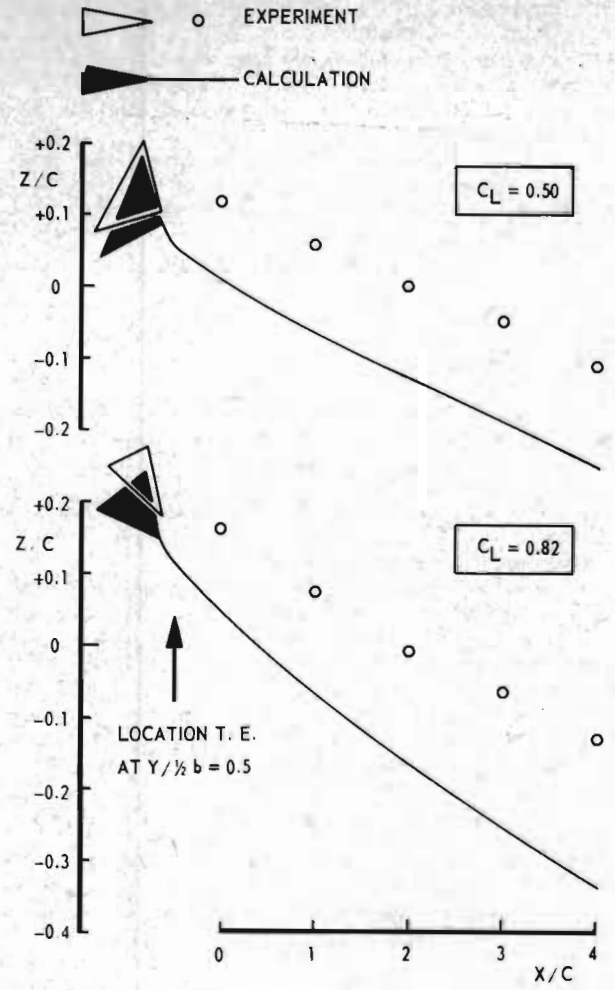

Fig.16 Measured and calculated downstream wake location at mid semi span. Notice the difference in horizontal and vertical scale.

Part of the difference in downstream slope can be explained by tunnel wall constraint, as is shown in figure 17, where the measurements are corrected for tunnel wall constraint[10] and where the trailing edges at mid semi span are made to coincide. There remains a difference between calculation and measurement, which is partly caused by:

- The fact, that in viscous flow the trailing vorticity originates mainly from the boundary layer of the upper wing surface. Simultaneous measurements of total head and vorticity revealed[8] that the trailing vorticity is located above the centre of the total head wake.
- The different angles, at which the vortex sheet leaves the trailing edge in potential and viscous flow. According to the criteria of Mangler and Smith[11], valid for potential flow, the vortex sheet has (in the present case) to leave the wing in a direction parallel to the wing upper surface. Measurements in viscous flow showed[8], that at small incidence the wake leaves the wing in a direction approximately parallel to the bisector of the tail angle and at high incidence more or less parallel to the wing lower surface.

The calculated vortex sheet is strongly curved close behind the trailing edge. The influence of the initial direction of the vortex sheet on the vertical location further downstream, will probably be small.

6.5 Sidewash

Because the shape of the vortex sheet can only be approximately calculated, it is important to know, whether the downstream velocity field can be predicted with some accuracy.

The downwash is rather well predicted, because there is only a slight difference between calculated and measured slope of the downstream vortex sheet location, as is shown in figure 17. Examples of detailed calculations of the sidewash are given in the figures 18 and 19. The data labelled "first step" are calculated with straight trailing vortices approximately parallel to the wing chord. The "second step" data are calculated with the deformed vortex sheet (cf. Fig.15).

An inviscid continuous vortex sheet would show a discontinuity in the sidewash, when the

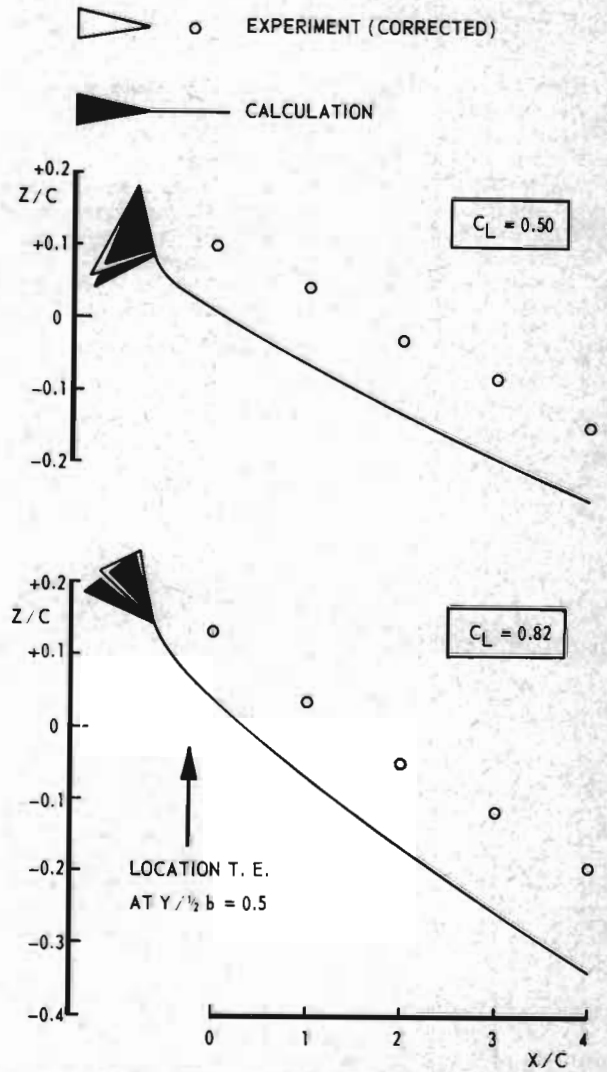

Fig.17 Measured and calculated downstream wake location at mid semi span. Measured location corrected for tunnel wall constraint and for difference in trailing edge position.

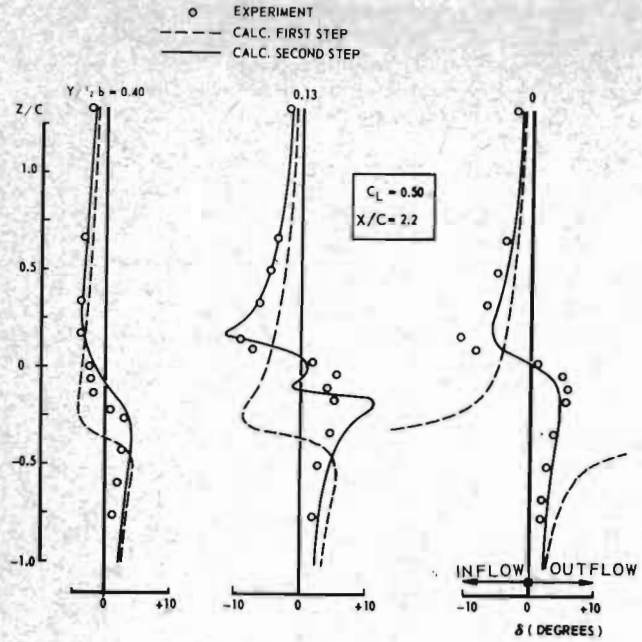

Fig.18 Measured and calculated values of the sidewash behind the wing at C_L = 0.50.

vortex sheet is crossed. With the discrete vortex representation, this discontinuity no longer exists, as long as the discrete vortex is not crossed. The sidewash distribution midway between the discrete vortices resembles (more or less accidentally) the sidewash distribution of the viscous vorticity layer. The second step improves the agreement in most cases.

The agreement between calculated and measured sidewash is in the tip region better at C_L = 0.50 than at C_L = 0.82, notwithstanding the remark stating the opposite in section 6.4, regarding the calculated downstream shape of the vortex sheet (cf. Fig.15). The large difference between calculation and measurement in Fig.19 at 2y/b = = 0.13, is caused by the concentrated tip vortex, present in the measurements.

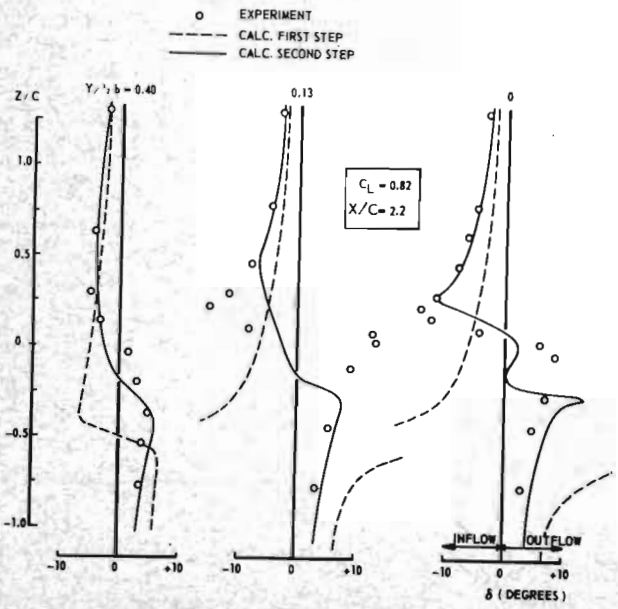

Fig.19 Measured and calculated values of the sidewash behind the wing at C_L = 0.82.

The present numerical method uses the velocity midway between discrete vortices, to determine the streamline pattern and thus the vortex sheet location. The good agreement between calculated and measured sidewash at some distance away from discrete or concentrated vortices (e.g. at 2y/b = 0.40) shows, that this choice works well within the range of discretizations applied in these calculations.

7. Concluding remarks

7.1 Experiment

At the trailing edge, about 60 percent of all trailing vorticity is already concentrated in a tip vortex, which originates in the boundary layer on the wing tip upper surface. The tip vortex flows downstream approximately parallel to the free-stream, without significant variation of its strength.

The remaining part of the trailing vorticity leaves the wing in the form of a vorticity layer. The inboard part moves downwards and the vorticity diffuses slowly into the surrounding air, whereas the outboard part of the vorticity layer moves in a helical path around the tip vortex, diffusing its vorticity into the surrounding air without concentrating it into the core of the tip vortex.

Except the trailing vorticity close to the tip vortex, the vorticity is located above the centre of the total-head wake of the wing. Therefore, the centre of the total-head wake is not a reliable measure for the location of the trailing vorticity.

7.2 Comparison of calculation and measurement

The spanwise lift distribution is well predicted, with the exception of a slight underestimation at the root. Other discrepancies are due to:

- Flow separation on the trailing edge at high lift,
- The tip vortex, already present upstream of the trailing edge on the wing tip upper surface, which was not represented in the mathematical model used.

The calculated influence of the deformation of the vortex sheet on the over-all lift, was about 3 percent.

The pressure distribution was also well predicted, even on the front part of the wing tip. The discrepancies in the pressure distribution on the rear part of the wing tip are possibly due to neglecting the flow separation on the tip and the corresponding tip vortex formation.

The vertical displacement of the vortex sheet is generally overestimated, except at the wing root. The main reason for this is the neglect of viscous effects in the calculations, viz.:

- In viscous flow, the trailing vorticity stems mainly from the wing upper surface and is, therefore, located in the upper part of the total-head wake behind the wing.
- The initial direction of the wake is not the same in potential and viscous flow. The criteria of Mangler and Smith are not applicable in viscous flow. The influence on the vertical location of the wake farther downstream, is possibly small.

There are discrepancies between the calculated and the measured shape of the vortex sheet. The discrepancies are not fully clarified, but have their roots in:

- The numerical iteration process. The influence of several computational details will possibly be investigated in the future.
- The neglect of viscous effects, i.e. the neglect of the concentrated vortex, already existing on the wing tip upper surface and the neglect of the diffusion of vorticity.

Notwithstanding the discrepancy between calculated and measured shape and position of the vortex sheet, the agreement between calculated and measured sidewash is satisfactory at distances not too close to discrete or concentrated vortices. This agreement also supports the choice made in this mathematical model, viz. to determine the path of the trailing vortices from velocities, calculated midway between the discrete vortices.

Apart from the discrepancies between measured and calculated shape and position of the vortex sheet, the present results are sufficiently accurate to predict for moderate lift, the flow around downstream aircraft components (e.g. tail surfaces), when the proximity to the tip region of the vortex sheet is not too close. Improvement of the mathematical model should in the first place concern the treatment of the tip flow.

References

1 Westwater, F.L., "Rolling Up of the Surface Discontinuity Behind an Aerofoil of Finite Span", A.R.C. R and M 1962, 1936.

2 Hancock, G.J., "On the Rolling Up of a Trailing Vortex Sheet", Aero. Journ., September 1970, pp. 749 - 752.

3 Hackett, J.E. and Evans, M.R., "Vortex Wakes Behind High-Lift Wings", Journ. of Aircr., Vol.8, No.5, May 1971, pp. 334 - 340.

4 Maskew, B., "The Calculation of Potential Flow Aerodynamic Characteristics of Combined Lifting Surfaces with Relaxed Wakes", H.S.A. Note No. YAD 3192, September 1973.

5 Labrujère, Th.E., "A Numerical Method for the Determination of the Vortex Sheet Location Behind a Wing in Incompressible Flow", NLR TR 72091 C, July 7th, 1972.

6 Labrujère, Th.E. and De Vries, O., "Evaluation of a Potential Theoretical Wake Model via Comparison of Measurements and Calculations", NLR TR 74063 C, 1974.

7 Labrujère, Th.E., Loeve, W. and Slooff, J.W., "An Approximate Method for the Calculation of the Pressure Distribution on Wing-Body Combinations at Subcritical Speeds", AGARD Conf. Proc. No.71, Paper No.11, September 1970.

8 De Vries, O., "Wind Tunnel Investigation of the Development of the Vortex Wake Behind a Sweptback Wing", NLR TR 72017 C, March 1973.

9 Dosanjh, D.S., Grasparek, E.P. and Eskinazi, S., "Decay of a Viscous Trailing Vortex", Aeron. Quart., Vol.13, 1962, p.167

10 Gillis, Clarence L, Polhamus, Edward C. and Gray Jr., Joseph L., "Charts for Determining Jet-Boundary Corrections for Complete Models in 7 by 10 foot Rectangular Wind Tunnels", NACA Wartime Report 486, 1945.

11 Mangler, K.W. and Smith, J.H.B., "Behaviour of the Vortex Sheet at the Trailing Edge of a Lifting Wing", R.A.E. TR 69049, March 1969.

DISCUSSION

A. Das (DFVLR-Braunschweig, Germany): In the picture of your paper, the spanwise circulation distribution of the rolled-up vortex sheet is shown. In case the vortex sheet is completely rolled up at the edges, how is the circulation distribution defined in the rolled-up area - both from experiment and theory? If we relate the circulation with the potential jump across the vortex sheet, the rolled-up area presents some formal difficulties.

O. de Vries: The circulation at a radius R from the centre of the tip vortex in figure 11 of the paper, is defined as the contour integral of the velocity tangential to a circle with radius R perpendicular to the free-stream.

The vortex indicator rotates due to tangential velocities and in that way measures the contour integral. The experimental determination of the circulation is difficult, especially of the effective radius of the vortex indicator.

The circulation distribution is not calculated, because of the limited number of discrete vortices used and because the calculated vortex sheet was not rolled up.